Low Current Vacuum Arc in Strong External Axial Magnetic Field

D.L. Shmelev

Institute of Electrophysics RAS, 620016 Ekaterinburg, Russia. E-mail: shmelev@iep.uran.ru

Abstract – The 2D magnetohydrodynamic model of the low current vacuum arc under action of strong axial magnetic field (AMF) is presented. It is supposed that modelled low current arc (LCA) is the part of high current vacuum arc, witch operate in multicathode spot mode and can be treated as the array of independently burning LCA.

1. Introduction

High-current vacuum arc with external axial magnetic field (B_{AMF}) exhibit different modes [1,2]. Their appearance depends mainly on the strength of B_{AMF} and arc current. At B_{AMF} strength approximately more then 10 mT/kA the vacuum arc exists in so called multi-cathode-spot (MCS) mode. The mode is characterized by the numerous well-defined cathode spots. These spots distributed homogeneously across the arc cathode root [3]. Each spot carries a relatively small current (~ 15 A). Plasma jets associated with the spots seem to behave independently, at least at moderate current. Because of it seems obviously to use the model of single plasma jet as the first approach to describing MCS mode. For the second step it is necessary to use certain model for overlapping of adjacent jets. This way was successfully used in work [4] for the model of the dependence of arc voltage on B_{AMF}.

In with work a model for low current vacuum arc in high external AMF is presented. In contrast to [4] a more comprehensive MHD approach was used for the modeling of single plasma jet originating from cathode spot. Overlapping of the jets is out of the topic of presented model, it will be done in the future modeling.

2. Model Formulation

Task geometry is shown on the Fig. 1, axial symmetry is assumed. It is considered the plasma jet originating from a group spot with an effective radius R_0. At the starting position the directed plasma velocity has a certain jet angle α. Anode is modeled as an equipotential surface with the anode sheath taken into account. Anode collects perfectly current and particle flow. External magnetic field has only axial component. Plasma stream has the free radial boundary whose position is determined us the part of self-consistent solution.

By analogy with [5] it is supposed that at the cathode boundary of calculated domain we already have a supersonic plasma stream. Characteristics of this stream are typical for the low current arc on a cupper cathode, i.e. drift plasma velocity u_i in order of 10^6 cm/s, average charge state Z – 1.85, electron temperature T_e – several eV, ion temperature T_i – less then 1 eV, erosion rate – 40 μg/C. Also at the cathode side an effective radius R_0 and jet angle α mast be specified. All mentioned values on the cathode boundary are the task parameters. Calculations in the present paper was done with the following parameters: current – 15 A, u_i – 106 cm/s, T_e – 2.5 eV, T_i – 0.5 eV, R_0 – 0.04 cm, α – π/8, and interelectrode gap L – 0.3 cm.

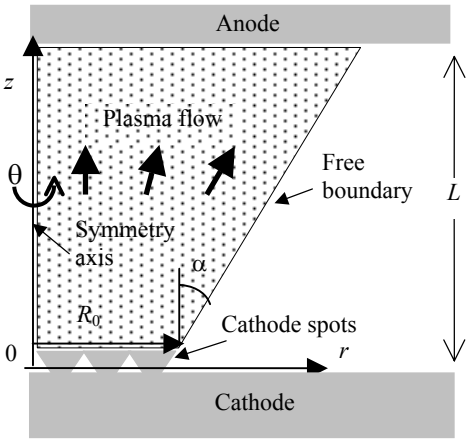

Fig. 1. Task geometry

In the interelectrode gap plasma flow is described by the set of MHD eqs. (1)–(10) [6].

$$\frac{\partial n_i}{\partial t} + \operatorname{div} n_i \vec{u}_i = 0; \tag{1}$$

$$m_i n_i \left(\frac{\partial \vec{u}_i}{\partial t} + \vec{u}_i \cdot \vec{\nabla} \vec{u}_i \right) = -\vec{\nabla}\left(n_e T_e + n_i T_i \right) + \frac{1}{c}\left[\vec{J} \times \vec{B} \right]; \tag{2}$$

$$\frac{3}{2} n_i \left(\frac{\partial T_i}{\partial t} + u_i \cdot \vec{\nabla} T_i \right) + n_i T_i \operatorname{div} \vec{u}_i = 3 \frac{m_e}{m} \frac{n_e}{\tau_{ei}} \left(T_e - T_i \right); \tag{3}$$

$$\frac{3}{2} n_e \left(\frac{\partial T_e}{\partial t} + \vec{u}_e \cdot \vec{\nabla} T_e \right) + n_e T_e \operatorname{div} \vec{u}_e + \operatorname{div} \vec{Q}_e =$$

$$= -3 \frac{m_e}{m} \frac{n_e}{\tau_{ei}} \left(T_e - T_i \right) + \frac{\vec{J}^2}{\sigma} + \frac{\beta}{e} \vec{J} \cdot \vec{\nabla} T_e; \tag{4}$$

$$\vec{Q}_e = \beta n_e T_e \left(\vec{u}_e - \vec{u}_i \right) - \gamma \frac{n_e T_e \tau_{ei}}{m_e} \vec{\nabla} T_e; \tag{5}$$

$$\frac{\partial B_\theta}{\partial t} + \frac{\partial u_{e,z} B_\theta}{\partial z} + \frac{\partial u_{e,r} B_\theta}{\partial r} - \frac{\partial u_{e,\theta} B_z}{\partial z} - \frac{\partial u_{e,\theta} B_r}{\partial r} =$$

$$= \frac{c^2}{4\pi} \left(\frac{\partial}{\partial r} \frac{1}{r \sigma_r} \frac{\partial r B_\theta}{\partial r} + \frac{\partial}{\partial z} \frac{1}{\sigma_z} \frac{\partial B_\theta}{\partial z} \right); \tag{6}$$

$$\frac{\partial A}{\partial t}+u_{e,z}\frac{\partial A}{\partial z}+u_{e,r}\frac{1}{r}\frac{\partial A}{\partial r}=\frac{c^2}{4\pi\sigma}\left(\frac{\partial}{\partial r}\frac{1}{r}\frac{\partial rA}{\partial r}+\frac{\partial^2 A}{\partial z^2}\right);(7)$$

$$\vec{J}=-\frac{c}{4\pi}\ \mathrm{rot}\,\vec{B},\ \vec{u}_e=\vec{u}_i-\frac{\vec{J}}{e\,n_e},\ n_e=Z\,n_i\,; \quad (8)$$

$$B_r=-\frac{\partial A}{\partial z},\ B_z=\frac{1}{r}\frac{\partial\, r\,A}{\partial r},\ \sigma_0=\frac{n_e e^2\tau_{ei}}{m_e}\,; \quad (9)$$

$$\sigma=\frac{\sigma_0}{1+\omega_{abn}\tau_{ei}},\ \omega_{abn}=10^{-2}\frac{T_e}{T_i}\frac{|u_e-u_i|}{u_s}\omega_{pi}\,. \quad (10)$$

For eqs. (3) and (6) on anode side we have the following nontrivial boundary condition:

$$2.5\ \ n_e\,u_{e,z}\,T_e+Q_{e,z}=n_e\,u_{e,z}\,T_e\left(2-\ln\frac{J_z}{J_{th}}\right); \quad (11)$$

$$\frac{J_r}{\sigma}+\left(\frac{J_z}{ecn_e}+\frac{u_z}{c}\right)B_\theta-\left(\frac{J_\theta}{ecn_e}+\frac{u_\theta}{c}\right)B_z+\frac{1}{en_e}\frac{\partial}{\partial r}n_eT_e=$$
$$=\frac{\partial}{\partial r}\left(\frac{T_e}{e}\ln\frac{J_z}{J_{th}}\right),J_{th}=\frac{1}{4}en_eu_{e,th}. \quad (12)$$

As can be seen from eqs. (3), (4) a two-temperature approach is used, and electron heat conduction (5) was taken into account. The depending of Braginskii coefficient γ and β on Z and AMF also was used. In the eq. (2) all three component of ion velocity are involved. Modification of AMF by the interaction with plasma jet is obtained from the eq. (7) for the θ-component of the vector potential. Also can be seen that depending of conductivity σ on AMF does not express explicitly. The fourth and fifth terms on the left hand side of eq. (6) are responsible for the action of AMF on the current density distribution. Equations (10) express that abnormal resistivity resulting from ion-sound instability [7] was taken into account. Set (1)–(12) was solved numerically in order to obtain steady state solution.

More detailed description of used equations and the method of numerical solution was done in [2], there similar equation set was used for modeling of high-current vacuum arc in diffusion mode.

3. Obtained Results

Typical spatial distributions of various plasma parameters across plasma jet are shown on Figs. 1–7. The value of externally applied AMF for shown result was 0.15 T. It can be seen that plasma flow differ considerably from simple spherical expansion in spite of the fact that free plasma boundary declines weakly from initial direction (Fig. 9). Axial magnetic field inside plasma jet is about 1% only below the applied AMF (Fig. 5). But just this small deviation of AMF provides the considerable value of azimuthal current (Fig. 3), and hence describes the interaction of external field with current flowing along the plasma jet.

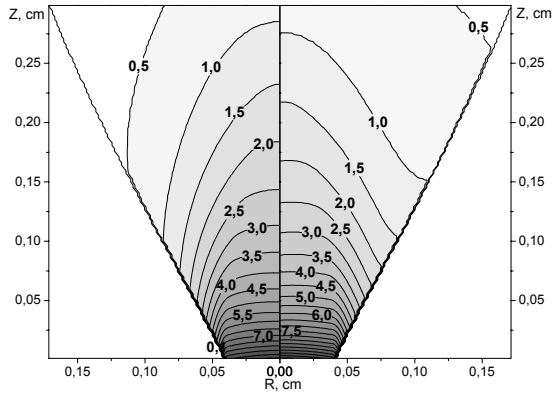

Fig. 2. Left side-pressure, mBar; right side – n_i, 10^{14} cm^{-3}

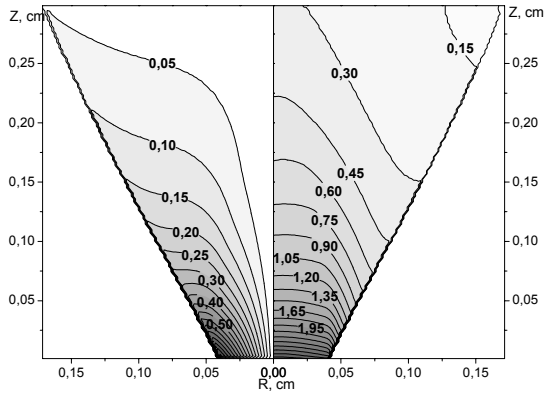

Fig. 3. Left side – azimuthal current density kA; right side – current density $S_{qrt}(J_r^2+J_z^2)$ kA

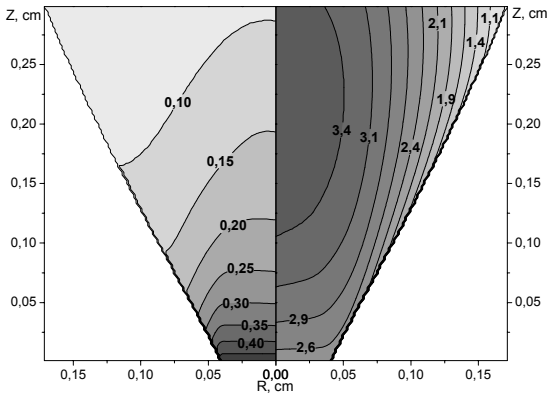

Fig. 4. Left side – T_i, eV; right side – T_e, eV

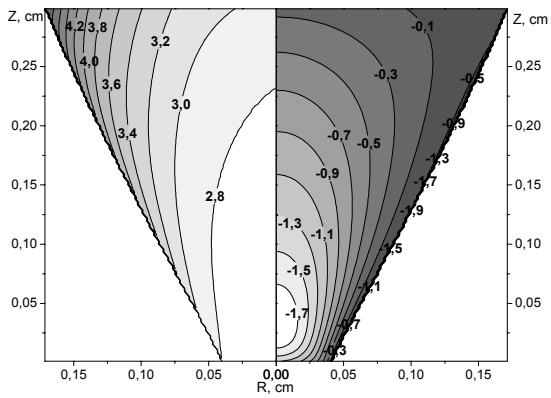

Fig. 5. Left side – Mach number; right side – deviation of magnetic field from external AMF: $S_{qrt}(B_r^2+B_z^2)-B_{AMF}$, mT

From Fig. 4 one can see that electron temperature considerably higher then ion temperature. In the course of plasma expansion the difference between electron and ion temperatures even grows. This condition together with high electron current velocity provides the good condition for development of ion-sound instability, witch in turn decrease electrical conductivity. Fig. 6 shows that abnormal resistivity mach higher then coulomb plasma resistivity. In the described case the effective conductivity close to anode is smaller then coulomb conductivity by a factor of 30. Such effect prevent the strong current constriction, witch must be without the additional resistivity due to both electron magnetization and presence of equipotential anode.

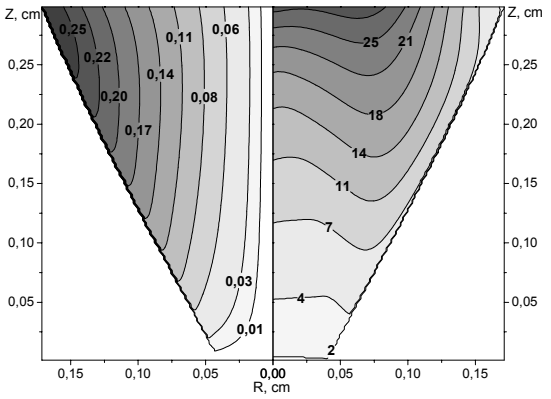

Fig. 6. Left side – rotational velocity 10^6 cm/s; right side – factor for decreasing conductivity due to instability

Plasma jet by the action of AMF obtains rotational velocity. Fig. 6 shows that such velocity is not small. High azimuthal ion velocity plays a significant role in the momentum balance.

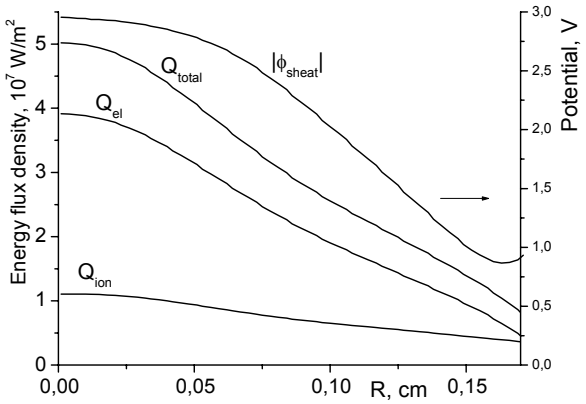

Fig. 7. Energy flux to anode and anode sheath potential

Radial distributions of energy flux densities are shown on Fig. 7. Mine contribution in total energy gives the electron flux. If we divide the integral of the total energy flux over anode area by total current (15 A), then we will obtain the effective anode voltage. In this case it will be about 12 V. With AMF increasing the maximum value of energy flux density increases (Fig. 8). This dependence is absolutely clear, because AMF increasing leads to plasma constriction (Fig. 9). Constriction, in turn, leads to the growth of current density and plasma heating.

Also the plasma voltage drop grows together with AMF (Fig. 10). Here the main role again plays the current constriction, and the decreasing of the absolute value of negative electron pressure gradient gives effect. Potential calculation was started from initial value –15 V, which approximately corresponds to voltage fall in cathode spot. Sharp negative drop on Fig. 10 is the voltage fall connected with anode sheath. Radial distribution of the absolute value of anode sheath voltage is shown on Fig. 7.

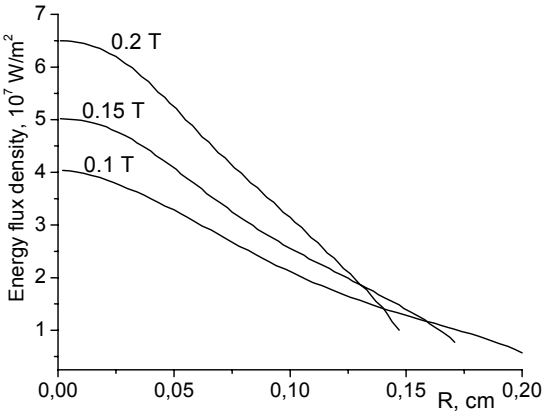

Fig. 8. Energy flux to anode at different AMF values

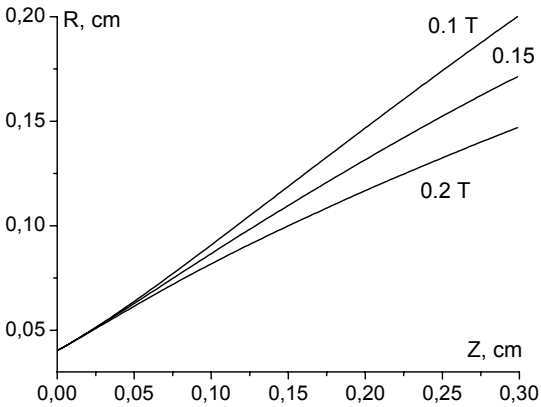

Fig. 9. Position of free plasma boundary at different AMF values

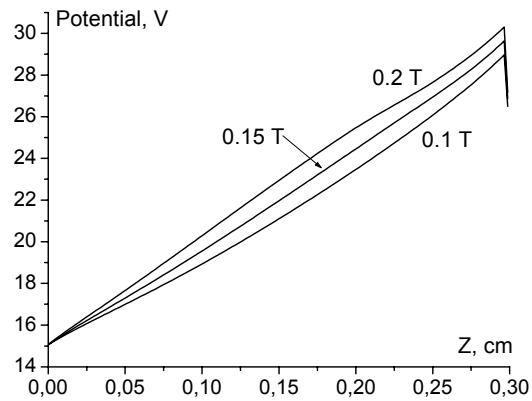

Fig. 10. Potential distribution along jet axis at different AMF values

In principle, in previous works ([4], [5] for example) qualitatively the same effects mentioned here were obtained. But presented model is more comprehensive, involves many important process witch was skipped in previous simple models, and therefore more suitable for the deep quantitative researching of MCS vacuum arc.

4. Conclusions

The computational model has been constructed to calculate the action of the strong axial magnetic field on plasma jet originating from group cathode spot. It was shown, in the parameter range investigated, that conditions for developing of ion-sound instability are fulfilled. The associated with instability abnormal resistivity is math higher then coulomb plasma resistivity. Calculations showed also that the maximum value of energy flux density to the anode increases with AMF increasing.

References

[1] M.B. Schulman and H. Schellekens, IEEE Trans. Plasma Sci. **28**, No. 2, 443–452 (2000).

[2] E. Schade and D. Shmelev, IEEE Trans. on Plasma Science **31**, 890–901 (2003).

[3] A.M. Chaly, A.A. Logatchev, S.M. Shkol'nik and K.K. Zabello, *in: Proc. XIXth Int. Symposium on Discharges and Electrical Insulation in Vacuum*, Xi'an, China, 2000.

[4] M. Keidar and M.B. Schulman, IEEE Trans. Plasma Sci. **29**, No. 5, 684–689 (2001).

[5] M. Keidar, I. Beilis, R.L Boxman, and S. Goldsmith, J. Phys. D: Appl. Phys. **29**, 1973–1983 (1996).

[6] S.I. Braginskii, *in: Reviews of Plasma Physics*, M.A. Leontovich, Editor, New York: Consultants Bureau, 1965.

[7] V.V. Vikhrev and V.M. Korzhavin, Plasma Physics (in Russian) **4**, 735–745 (1978).